Nonlinear Control Law Design for Inverted Pendulum Systems via RBF Neural Networks

Huynh Van Khuong [1], Nguyen Xuan Chiem [2,*], Alexander Obukhov [3]
[1,2] Department of Automation and Computing Techniques, Le Quy Don Technical University, Hanoi, Vietnam
[3] Don State Technical University, 1, Gagarin Square, Rostov-on-Don 344000, Russia
Email: [1] huynhvankhuong93@gmail.com, [2] chiemnx@mta.edu.vn, [3] pobuhov@spark-mail.ru
*Corresponding Author

***Abstract*—This paper presents the design of a nonlinear control law based on the Backstepping method combined with Radial Basis Function (RBF) neural networks to ensure the stability of an inverted pendulum system with unknown model parameters. The control design is developed using a general form of the system's mathematical model, in which the unknown nonlinear functions are approximated by RBF neural networks. Experimental results conducted on the STM32F4 embedded platform demonstrate that the proposed approach not only guarantees system stability but also verifies the effectiveness and practical applicability of the control law.**

***Keywords*—Backstepping; RBF Neural Networks; Adaptive Control; Inverted Pendulum System**

I. INTRODUCTION

The inverted pendulum represents one of the most fundamental and challenging problems in nonlinear control due to its inherent instability, strong nonlinearity, and high-order dynamics. This system has a wide range of industrial applications, including two-wheeled self-balancing vehicles (e.g., Segways), rockets, spacecraft, intelligent robots, and various systems that model crane mechanisms. The primary control objective is to stabilize the pendulum in its inherently unstable upright position while simultaneously controlling the position of the cart. Achieving this objective requires control strategies that are not only precise but also robust and adaptive to model uncertainties.

Numerous studies have investigated the stable control of the inverted pendulum system using a variety of control laws [1]-[6]. Traditional control algorithms, such as the Proportional-Integral-Derivative (PID) controller [1], are generally inadequate for handling the system's complex and nonlinear dynamics, as they are unable to effectively address inherent uncertainties and external disturbances. Furthermore, the system's robust stability degrades in the presence of parameter and structural uncertainties, making gain tuning in PID controllers a particularly challenging task [2]. These limitations underscore the need for more advanced control strategies, such as the Linear Quadratic Regulator (LQR) [3]-[6]. However, the performance of LQR significantly deteriorates when the system operates far from the equilibrium point or under model uncertainties.

To address these limitations, nonlinear control techniques have been proposed [8]-[20]. Feedback linearization has been applied in various studies [8], [9], while sliding mode control laws have also been developed [10], [11]. The Backstepping method has been employed to design stable controllers based on accurate system models [12], and other works have introduced control strategies grounded in synergetic theory control [13]-[15]. These approaches aim to ensure system stability and robustness against model uncertainties. In general, nonlinear control methods enhance system stability and improve disturbance rejection. Additionally, adaptive control strategies are commonly used to handle parameter uncertainties, while intelligent control approaches—including fuzzy logic, neural networks, and reinforcement learning-show significant promise in managing complex dynamic systems without requiring precise mathematical models [16]-[22]. In this study, a control approach is proposed based on a general mathematical representation of the system, under the assumption that the exact parameters of the system model are unknown. The Backstepping method is initially employed to design a control law for the inverted pendulum using the general form of the system's dynamics. To approximate the unknown components of the model, four Radial Basis Function (RBF) neural networks are utilized, each corresponding to a specific nonlinear function within the system. This framework enables the design of a control law that does not rely on precise knowledge of the system dynamics, while still guaranteeing the asymptotic stability of the overall system.

The structure of this paper is organized as follows: Section 2 presents a general mathematical model of a two degrees-of-freedom underactuated mechanical system. Section 3 describes the design of the Backstepping control law based on Radial Basis Function (RBF) neural networks. Section 4 introduces the experimental model of the inverted pendulum and discusses the experimental results obtained by implementing the proposed control law on the actual system. Finally, conclusions and directions for future research are provided in Section 5.

II. MATHEMATICAL MODEL OF THE 2-DOF UNDERACTUATED MECHANICAL SYSTEM AND THE INVERTED PENDULUM MODEL

To derive the equations of motion for mechanical systems, the Lagrangian method is employed. The Lagrangian function (L) of a mechanical system [20] is defined as the difference between its total kinetic energy (T) and potential energy (P). The system's equations of motion are then obtained from the Lagrangian function using the Euler-Lagrange equations, as follows:

$$\frac{d}{dt}\left(\frac{\partial L}{\partial q}\right) - \frac{\partial L}{\partial q} = \tau \quad (1)$$

Where: q represents the generalized coordinates, and τ is the generalized torque vector. In the case of a mechanical system composed of rigid bodies connected by joints, the kinetic energy is calculated as the sum of the kinetic energies of each rigid body. The kinetic energy of each rigid body is decomposed into two terms: the first term results from the translational motion of the body's center of mass, and the second term arises from the rotational motion of the body about its inertia center. The potential energy is typically simplified to a term originating from gravitational forces. This term depends only on the position of the body's center of mass. Applying the Euler-Lagrange equations (1) yields equations that describe the evolution of the generalized coordinates over time. For a mechanical system consisting of rigid bodies, these equations take the following general form [9], [20]:

$$M(q)\ddot{q} + C(q,\dot{q})\dot{q} + G(q) = \tau = R(q)u \tag{2}$$

The symmetric positive-definite matrix $M(q) \in R^{n\times n}$ is called the inertia matrix of the mechanical system. In the general case, it depends on the configuration q of the mechanical system. The matrix $C(q,\dot{q}) \in R^{n\times n}$ corresponds to the centrifugal and Coriolis forces and depends on both the configuration q and the generalized coordinate velocities $\dot{q}$. The vector $G(q) \in R^n$ corresponds to gravity and depends only on the configuration q. τ is the torque vector of the actuators.

The matrix $R(q) \in R^{n\times m}$ represents the distribution of forces over the generalized coordinates. And $u \in R^m$ is the input vector of the actuators. A mechanical system is called underactuated if rank$\{R(q)\} < n$, meaning the system has fewer independent control inputs than degrees of freedom. Suppose the following holds: $[r\ (1-r)]^T u$, where r = 1 or 0 and u is the control signal.

For the inverted pendulum system, which is a 2-DOF underactuated mechanical system illustrated in Fig. 1, let $x_1 = q_1$ denote the position of the cart, and $x_2 = q_2$ denote the angle of the pendulum (with $x_2 = 0$ when the pendulum is upright, and $x_2 = \pi$ when the pendulum is downward), x_3 be the velocity of the cart, and x_4 be the angular velocity of the pendulum. The state of the inverted pendulum system is represented by the vector $x = [x_1, x_2, x_3, x_4]^T$. From equation (2), after transformation, the state-space equations describing the inverted pendulum system take the following form:

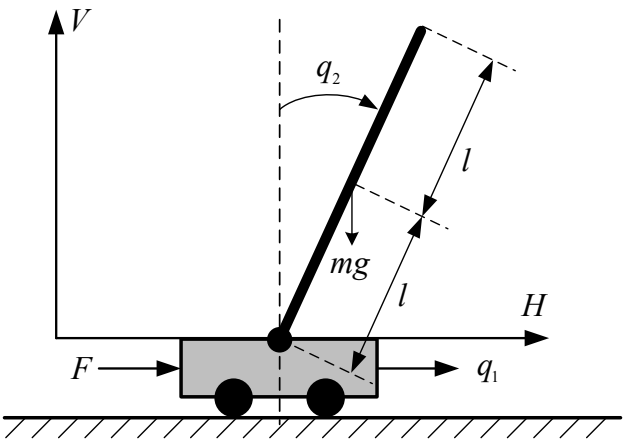

Fig. 1. Inverted pendulum system model

$$\begin{cases} \dot{x}_1 = x_3 \\ \dot{x}_2 = x_4 \\ \dot{x}_3 = f_3(x) + g_3(x)u_t \\ \dot{x}_4 = f_4(x) + g_4(x)u_t \end{cases} \tag{3}$$

Where u_t is the voltage supplied to the motor that generates force acting on the cart, and $f_3(x)$, $g_3(x)$, $f_4(x)$, and $g_4(x)$ are functions containing unknown dynamic components.

III. Synthesis of Adaptive Backstepping Control Law Based on RBF Neural Networks

A. Steps to Synthesize a Stable Backstepping Control Law for the Balancing Pendulum Based on Mathematical Model (3)

Step 1: Define

$$e_1 = x_2 - k_1 x_1 \tag{4}$$

Where k_1 is a constant, taking the derivative of (4), we have:

$$\dot{e}_1 = \dot{x}_2 - k_1\dot{x}_1 = x_4 - k_1 x_3 \tag{5}$$

To achieve the objective $e_1 \to 0$, the Lyapunov function is chosen as follows:

$$V_1 = (1/2)e_1^2 \tag{6}$$

Taking the derivative of the Lyapunov function (6), we have:

$$\dot{V}_1 = e_1\dot{e}_1 = e_1(x_4 - k_1 x_3) \tag{7}$$

To ensure system stability, that is $\dot{V}_1 \le 0$, we choose:

$$x_4 = -c_1 e_1 + k_1 x_3 \tag{8}$$

From condition (8) and expression (7), we have:

$$\dot{V}_1 = -c_1 e_1^2 \le 0 \tag{9}$$

Step 2: To satisfy expression (8), we select the virtual control signal in the form of:

$$x_{4d} = -c_1 e_1 + k_1 x_3 \tag{10}$$

With the objective of ensuring $x_4 \to x_{4d}$, the error between the actual and virtual signals is given by:

$$e_2 = x_4 - x_{4d} = x_4 + c_1 e_1 - k_1 x_3 \tag{11}$$

Derivative of expression (11):

$$\begin{aligned} \dot{e}_2 &= \dot{x}_4 + c_1\dot{e}_1 - k_1\dot{x}_3 \\ &= u_t(g_4 - k_1 g_3) + f_4 - k_1 f_3 + c_1(x_4 - k_1 x_3) \end{aligned} \tag{12}$$

Choose the Lyapunov function as follows:

$$V_2 = (1/2)e_1^2 + (1/2)e_2^2 \tag{13}$$

Taking the derivative of the Lyapunov function (13), we have:

$$\dot{V}_2 = e_1\dot{e}_1 + e_2\dot{e}_2 \\ = e_1(e_2 - c_1e_1) + e_2\dot{e}_2 = -c_1e_1^2 + e_2(e_1 + \dot{e}_2) \quad (14)$$

To ensure $\dot{V}_2 \leq 0$, we choose:

$$e_1 + \dot{e}_2 = -c_2e_2 \quad (c_2 > 0) \quad (15)$$

From equation (15), the control law is derived as follows:

$$u_t = \frac{1}{g_4 - k_1g_3}[k_1f_3 - f_4 - c_1(x_4 - k_1x_3) - e_1 - c_2e_2] \quad (16)$$

According to Lyapunov stability theory, e_1 and e_2 converge to zero.

To ensure the system converges to the desired stable state, a design constant k_2 needs to be added to adjust the value of the state variable x_1, i.e., $x_1' = k_2x_1$. Here, x_1' is the input signal applied to the control law (16) replacing x_1 to ensure $x_1 \to 0$.

To implement the control law (16), accurate model information is required. In other words, the specific mathematical expressions of the functions f_3, g_3, f_4, and g_4 must be known. In this study, the authors choose a solution that does not involve explicitly constructing these functions. Instead, these functions are identified through RBF neural networks based on the system states. The control law (16) is rewritten as follows:

$$u_t = \frac{1}{\hat{g}_4 - k_1\hat{g}_3}[k_1\hat{f}_3 - \hat{f}_4 - c_1(x_4 - k_1x_3) - e_1 - c_2e_2] \quad (17)$$

Where $\hat{f}_3$, $\hat{g}_3$, $\hat{f}_4$, and $\hat{g}_4$ are the estimates of f_3, g_3, f_4, and g_4, respectively.

If $\hat{f}_3 = f_3$, $\hat{g}_3 = g_3$, $\hat{f}_4 = f_4$, and $\hat{g}_4 = g_4$ then $\dot{V}_2 \leq 0$.

The unknown functions $\hat{f}_3$, $\hat{g}_3$, $\hat{f}_4$, and $\hat{g}_4$ can be approximated by neural networks. Fig. 2 shows the closed-loop adaptive control scheme based on RBF neural networks. Four RBF networks are used to approximate the functions f_3, g_3, f_4, and g_4 as follows:

$$\begin{cases} f_3 = W_1^Th_1 + \varepsilon_1; & g_3 = W_2^Th_2 + \varepsilon_2 \\ f_4 = W_3^Th_3 + \varepsilon_3; & g_4 = W_4^Th_4 + \varepsilon_4 \\ i = 1,2,3,4 \end{cases} \quad (18)$$

Where W_i is the ideal network weight vector, h_i is the Gaussian function, and ε_i is the approximation error.

$$\begin{cases} \hat{f}_3 = \widehat{W}_1^Th_1 = \widehat{W}_1^T\, exp\left(-\frac{\|x - c_j\|^2}{2b_j^2}\right) \\ \hat{g}_3 = \widehat{W}_2^Th_2 = \widehat{W}_2^T\, exp\left(-\frac{\|x - c_j\|^2}{2b_j^2}\right) \\ \hat{f}_4 = \widehat{W}_3^Th_3 = \widehat{W}_3^T\, exp\left(-\frac{\|x - c_j\|^2}{2b_j^2}\right) \\ \hat{g}_4 = \widehat{W}_4^Th_4 = \widehat{W}_4^T\, exp\left(-\frac{\|x - c_j\|^2}{2b_j^2}\right) \end{cases} \quad (19)$$

Where: $x = [x_1, x_2, x_3, x_4]^T$ is the input vector, $c_j = [c_{j1}, c_{j2}, \ldots, c_{jn}]$ is the center coordinate vector of the j-th neural network, $b_j = [b_1, b_2, \ldots, b_m]$ is the width vector of the Gaussian function, and $\widehat{W}_i^T$ is the estimated weight value. The block diagram with control law (17) using neural network (18) is shown in Fig. 2.

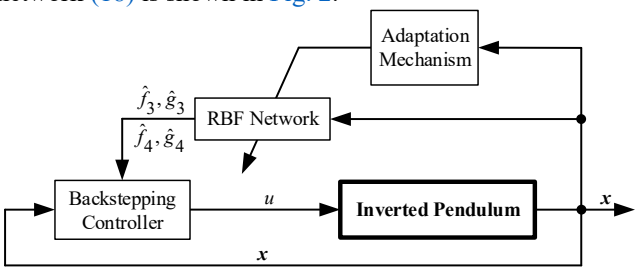

Fig. 2. Stabilizing control scheme based on RBF neural networks

The implementable adaptive law is presented in study [9]:

$$\dot{\hat{Z}} = \Gamma h\xi^T - n\Gamma\|\xi\|\hat{Z} \quad (20)$$

Where: $\hat{Z} = \begin{bmatrix} \widehat{W}_1 & 0 & 0 & 0 \\ 0 & \widehat{W}_2 & 0 & 0 \\ 0 & 0 & \widehat{W}_3 & 0 \\ 0 & 0 & 0 & \widehat{W}_4 \end{bmatrix}$ is the estimated weight matrix; $\Gamma = \begin{bmatrix} \Gamma_1 & 0 & 0 & 0 \\ 0 & \Gamma_2 & 0 & 0 \\ 0 & 0 & \Gamma_3 & 0 \\ 0 & 0 & 0 & \Gamma_4 \end{bmatrix}$ is a positive definite matrix of appropriate dimension; $\xi = [e_1\ e_2\ e_1\ e_2]^T$; $h = [h_1\ h_2\ h_3\ h_4]^T$; and n is a positive scalar.

B. Synthesis of Swing-Up Control Law

The control laws (17) themselves can only maintain the pendulum balance at the desired unstable equilibrium state $x = [0,0,0,0]^T$ if the initial state x_0 is within the neighborhood of x. This is because if the initial state x_0 is far from x, the closed-loop system will enter an unstable region or the control signal u_t impractical values. Therefore, it is necessary to use the Swing-up control law to bring the pendulum from the initial position with $x_2 = \pi$ to the vicinity of $x_2 = 0$. Afterwards, the control law (17) is employed to maintain the pendulum balance at the desired unstable equilibrium state.

Physically, for the pendulum to approach the vicinity of $x_2 = 0$, it must be supplied with energy, and its total energy must increase over time. Suppose at the initial state $x_0 = [0, \pi, 0,0]^T$, the pendulum has total energy $A = 0$. The energy components, including the kinetic energy T and potential energy V of the pendulum are calculated as follows:

$$T = \frac{1}{2}(J + ml^2)\dot{q}_2^2 \quad (21)$$

$$V = mgl(1 - cos(\pi - q_2)) \quad (22)$$

$$A = \frac{1}{2}(J + ml^2)\dot{q}_2^2 + mgl(1 - cos(\pi - q_2)) \quad (23)$$

The desired energy to be achieved by the pendulum when $x_2 = 0$ is:

$$A_0 = mgl(1 - cos(\pi - q_2)) = 2mgl \quad (24)$$

Using the proportional control technique, the control expression is determined as follows:

$$u = k_s(A_0 - A)sign(\dot{q}_2 cos(\pi - q_2)) \quad (25)$$

where k_s is the adjustment coefficient.

To simplify the implementation of the control law on the physical system, the control action is activated only when $A_0 - A > 0$. This implies that the control law (25) is applied only when $\pi/2 < q_2 \leq \pi$ with $\dot{q}_2 \geq 0$, and $-\pi \leq q_2 < -\pi/2$ with $\dot{q}_2 \leq 0$, under a fixed motor input voltage of 3 V. Therefore, a simplified version of the control law is presented in Fig. 3.

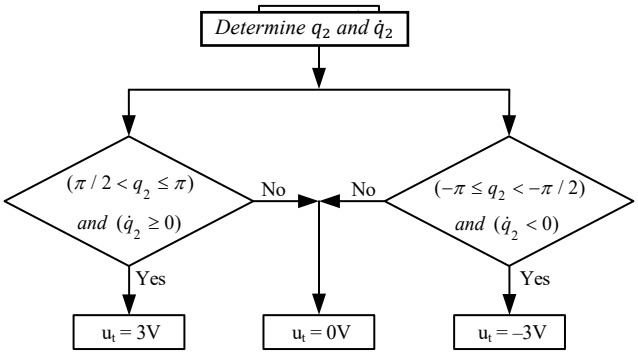

Fig. 3. Simple swing-up algorithm

IV. Experimental Results

In this experimental section, the aim is to verify the control law designed using the adaptive Backstepping method based on RBF neural networks (17), with the primary objective of bringing the pendulum angle $q_2 = 0$ within the limited travel range of the cart. Therefore, the cart's return to its initial position is not emphasized. Attempting to adjust the cart to return to the initial position would affect the objective of bringing the pendulum angle to zero, meaning the quality of the pendulum angle response would deteriorate. The initial angle for applying control laws (16) and (17) is $|q_2| = \pi/12(rad)$.

A. Experimental Model and Data Acquisition Software

The control law is executed on a real-time embedded system using a model self-built by the authors with the following system parameters: travel length of 0.4 m, pendulum mass variable, and cart mass of 712 g. The cart is driven by a ball screw transmission system and a DC motor. The components of the inverted pendulum control system are shown in Fig. 4. The STM32F407 microcontroller is used as the central processor, operating at a quartz frequency of 100 MHz. An encoder measuring the inverted pendulum angle (with a resolution of 600 pulses per revolution) and an encoder measuring the cart position (with a resolution of 100 pulses per revolution) are connected to the microcontroller. The DC motor is controlled via a controller and an H-bridge BTS7960 43 A circuit. The system is powered by a 12 V DC power supply with a current 10A. The system connects to data acquisition software through a UART serial communication port. The software, developed by the authors using C# on Visual Studio, allows observation of angle and position values by displaying numerical and graphical outputs on the screen.

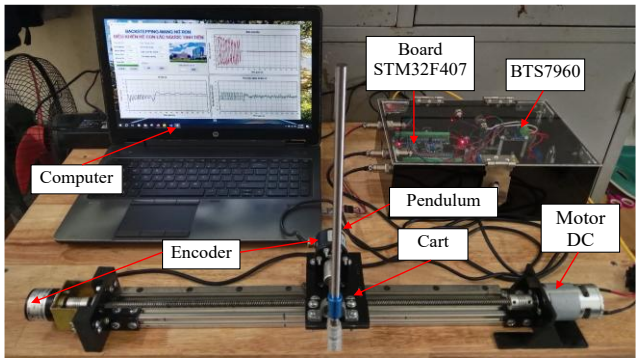

Fig. 4. Experimental model of the inverted pendulum on a cart system

The data acquisition software interface is shown in Fig. 5, with a data sampling period of 100 *ms*, featuring the following main functional groups: "States" displays the values of the state variables of the inverted pendulum system. "Graph" allows plotting or clearing graphs with two buttons labeled "DRAW" and "CLEAR". "Position Control" is used to control the cart position after balancing the pendulum at an angle $q_2 \approx 0$. The software interface displays time-based graphs of the system states, including Pendulum angle, Cart position, and Control signal u_t.

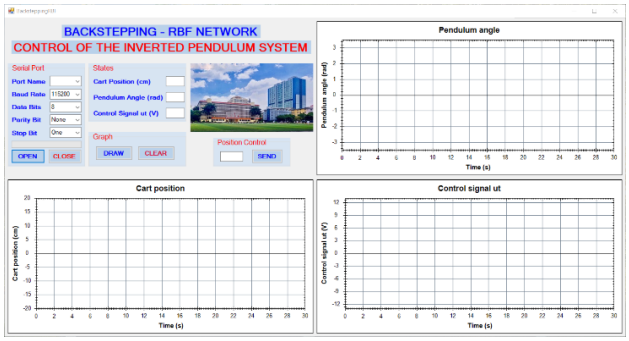

Fig. 5. Data acquisition software interface

B. Experimental Results

To demonstrate the effectiveness of the proposed control law (16) with the adaptive law (17) based on RBF neural networks, the authors conducted experiments under different scenarios with varying pendulum masses.

1. In case 01, the pendulum is a circular rod with a mass of 84 g. The response of the inverted pendulum system is shown in Fig. 6, Fig. 7, and Fig. 8.

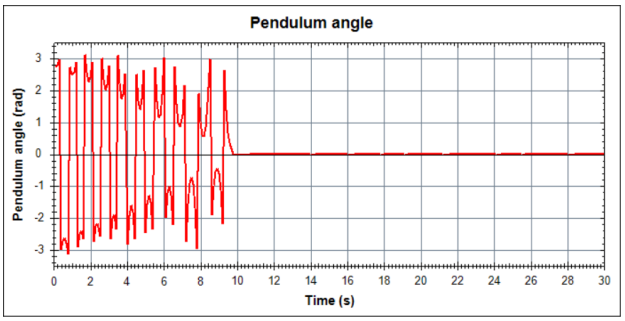

Fig. 6. Inverted pendulum angle response

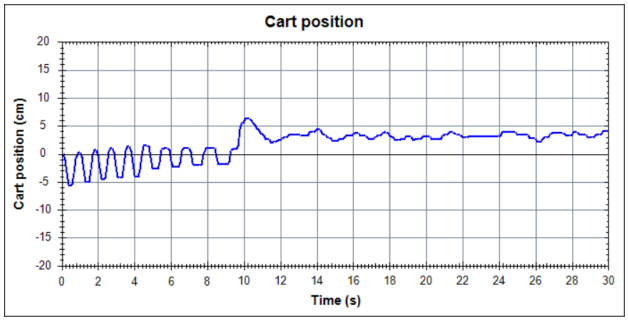

Fig. 7. Cart position response

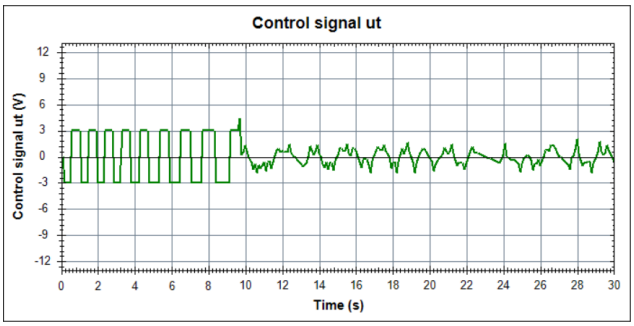

Fig. 8. System control signal

From the experimental results in this case, we observe that the proposed control law ensures the pendulum remains stable at the equilibrium position, but with some deviation in the cart position. From Fig. 6, it can be seen that the pendulum angle quickly approaches and stabilizes at the upright position within approximately 0.4 seconds starting from the angle $\theta = \pi/12\ rad$ Fig. 7 shows the cart position stabilizing at 3 cm with minimal oscillation. From Fig. 8, the control signal of the proposed control law remains within allowable limits and exhibits a low oscillation frequency.

2. In case 02, the pendulum is a circular rod with a mass of 126 g. The response of the inverted pendulum system is shown in Fig. 9, Fig. 10, and Fig. 11.

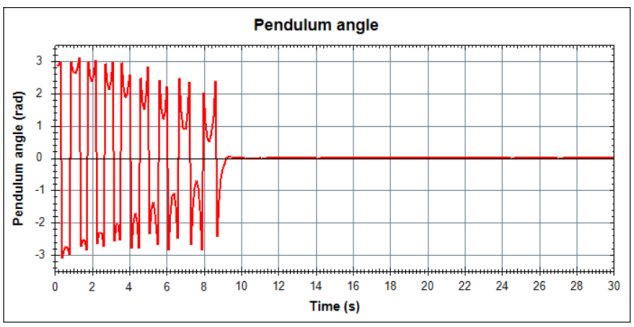

Fig. 9. Inverted pendulum angle response

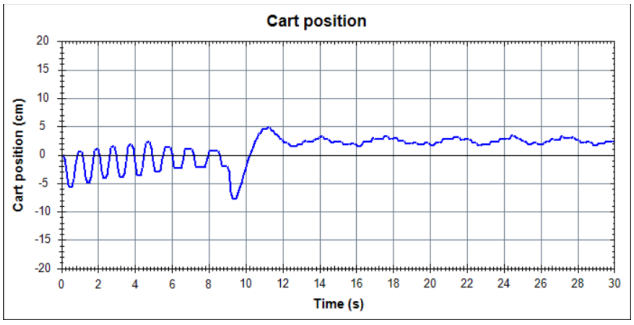

Fig. 10. Cart position response

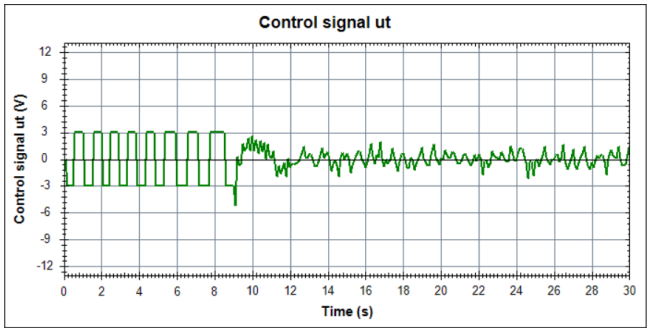

Fig. 11. System control signal

In this case, although the mass increases, the proposed control law still ensures the inverted pendulum remains stable at the upright position. However, Fig. 10 shows that the cart position oscillates periodically around 3 cm. Fig. 9 illustrates that the pendulum angle quickly approaches and stabilizes at the upright position within approximately 0.4 seconds. The control signal (Fig. 11) varies at a higher frequency compared to the first case.

3. In case 03, the pendulum is a circular rod with an attached load block, with a total mass of 502 g. The response of the inverted pendulum system is shown in Fig. 12, Fig. 13, and Fig. 14.

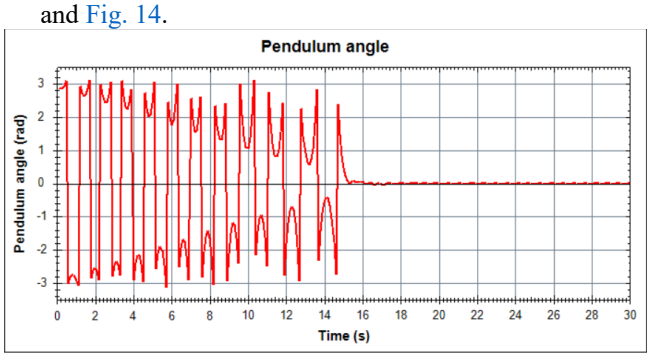

Fig. 12. Inverted pendulum angle response

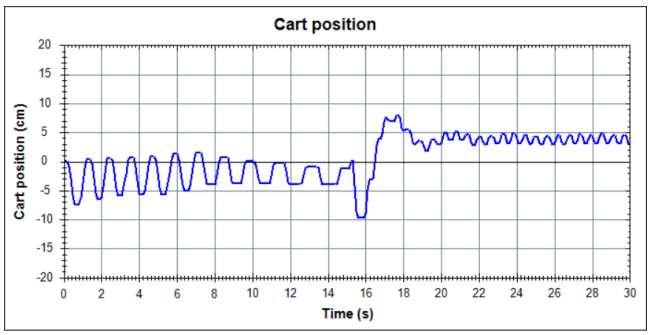

Fig. 13. Cart position response

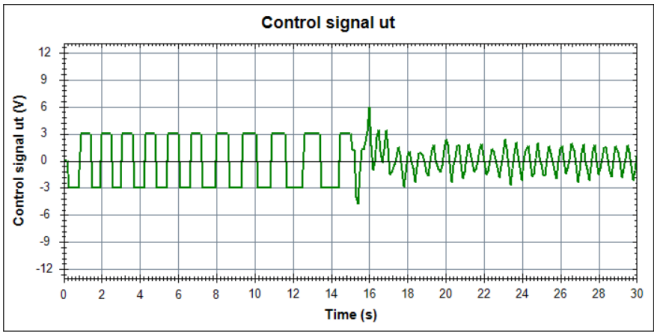

Fig. 14. System control signal

In this case, when the pendulum mass increases significantly, the time required to bring the pendulum close to the equilibrium point using the Swing-up controller increases to 14.4 seconds. The settling time to the equilibrium position, measured from the angle $\theta = \pi/12\ rad$, remains nearly unchanged, while small oscillations appear simultaneously (Fig. 12). From Fig. 13, we observe that the larger pendulum mass results in greater amplitude and stronger oscillations in the cart's movement compared to the previous two cases. The control signal (Fig. 14) also exhibits larger operating amplitude and stronger oscillations.

V. CONCLUSION

The authors of this paper proposed a method for designing a nonlinear control law to stabilize the inverted pendulum system using Backstepping control combined with RBF neural networks. The backstepping controller was developed based on the general mathematical model of a 2-DOF underactuated mechanical system. By leveraging the nonlinear function approximation capability of the RBF network to estimate the unknown functions in the model, experimental results under various conditions demonstrated that the system could maintain the pendulum in the upright position with low overshoot and fast response. This study not only confirms the effectiveness of the proposed control law for the inverted pendulum system but also suggests its potential applicability to any system that can be modeled in the form of an inverted pendulum. However, the results also reveal certain limitations, such as the cart position not returning to zero and the presence of oscillations when the model parameters vary significantly. In future work, the authors plan to apply intelligent techniques to optimize controller parameters and RBF network structures to enhance control performance.

REFERENCES

[1] L. B. Prasad, B. Tyagi, and H. O. Gupta, "Optimal control of nonlinear inverted pendulum system using PID controller and LQR: performance analysis without and with disturbance input," *International Journal of Automation and Computing*, vol. 11, no. 6, pp. 661-670, 2014, https://doi.org/10.1007/s11633-014-0818-1.

[2] T.-B. Dang *et al*., "PID Control for Cart and Pole system: Simulation and Experiment," *Journal of Fuzzy Systems and Control*, vol. 2, no. 1, pp. 29-35, 2024, https://doi.org/10.59247/jfsc.v2i1.165.

[3] N. X. Chiem and L. T. Thang, "Synthesis of LQR Controller Based on BAT Algorithm for Furuta Pendulum Stabilization," *Journal of Robotics and Control (JRC)*, vol. 4, no. 5, pp. 662-669, 2023, https://doi.org/10.18196/jrc.v4i5.19661.

[4] Fahmizal, Geonoky, and H. Maghfiroh, "Rotary Inverted Pendulum Control with Pole Placement," *Journal of Fuzzy Systems and Control*, vol. 1, no. 3, pp. 90-96, 2023, https://doi.org/10.59247/jfsc.v1i3.152.

[5] C. X. Nguyen, T. D. Pham, A. D. Lukynov, P. C. Tran, and Q. D. Truong, "Design embedded control system based controller of the quasi time optimization approach for a magnetic levitation system," *IOP Conference Series: Materials Science and Engineering*, vol. 1029, no. 1, p. 012020, 2021, https://doi.org/10.1088/1757-899X/1029/1/012020.

[6] D.-P. Hoang, "A Survey of Experimental LQR for Cart and Pole," *Journal of Fuzzy Systems and Control*, vol. 2, no. 2, pp. 97-103, 2024, https://doi.org/10.59247/jfsc.v2i2.211.

[7] C. N. Xuan and T. Le Tran, "Design of State Feedback Controller with Optimal Parameters Using Bat Algorithm for Reaction Wheel Pendulum," *2021 International Conference on Advanced Technologies for Communications (ATC)*, pp. 172-177, 2021, https://doi.org/10.1109/ATC52653.2021.9598306.

[8] N. X. Chiem and H. N. Phan, "Design controler of the quasi-time optimization approach for stabilizing and trajectory tracking of inverted pendulum," *MATEC Web of Conferences*, vol. 226, p. 02007, 2018, https://doi.org/10.1051/matecconf/201822602007.

[9] H. N. Phan and C. X. Nguyen, "Building embedded quasi-time-optimal controller for two-wheeled self-balancing robot," *MATEC Web of Conferences*, vol. 132, p. 02005, 2017, https://doi.org/10.1051/matecconf/201713202005.

[10] S. Irfan, A. Mehmood, M. T. Razzaq, and J. Iqbal, "Advanced sliding mode control techniques for inverted pendulum: Modelling and simulation," *Engineering science and technology, an international journal*, vol. 21, no. 4, pp. 753-759, 2018, https://doi.org/10.1016/j.jestch.2018.06.010.

[11] M. Mahmoud, R. Saleh, and A. Ma'arif, "Stabilizing of inverted pendulum system using Robust sliding mode control," *International Journal of Robotics and Control Systems*, vol. 2, no. 2, pp. 230-239, 2022, https://doi.org/10.31763/ijrcs.v2i2.594.

[12] H.-G.-B. Pham, "Trajectories Tracking Control for Rotary Inverted Pendulum using Backstepping Method," *Journal of Fuzzy Systems and Control*, vol. 3, no. 1, pp. 57-63, 2025, https://doi.org/10.59247/jfsc.v3i1.276.

[13] C. Nguyen, H. Phan, and H. Nguyen, "An energy saving method of stable control of inverted pendulum system when affected by external interference using auxiliary pendulum," *E3s web of conferences*, vol. 104, p. 5, 2019, https://doi.org/10.1051/e3sconf/201910401015.

[14] C. X. Nguyen, A. D. Lukianov, T. D. Pham, and A. D. Nguyen, "Synthesis of a nonlinear control law with efficiency energy for the self-balancing two wheeled vehicle," *IOP Conference Series: Materials Science and Engineering*, vol. 900, no. 1, p. 012002, 2020, https://doi.org/10.1088/1757-899X/900/1/012002.

[15] C. X. Nguyen, T. T. Le, P. C. Tran, A. D. Lukianov, K. D. Truong, and T. D. Pham, "Synthesis of non-linear controller to energy efficiency for damped-elastic-jointed inverted pendulum," *E3S Web of Conferences*, vol. 279, p. 01020, 2021, https://doi.org/10.1051/e3sconf/202127901020.

[16] A. Jain, D. Tayal, and N. Sehgal, "Control of non-linear inverted pendulum using fuzzy logic controller," *International Journal of Computer Applications*, vol. 69, no. 27, pp. 7-11, 2013, https://doi.org/10.5120/12141-8278.

[17] J. Liu, "Radial Basis Function (RBF) Neural Network Control for Mechanical Systems," *Springer Nature Link*, 2013, https://doi.org/10.1007/978-3-642-34816-7.

[18] A. Bounemeur, M. Chemachema, and S. Bouzina, "Fuzzy Fault-Tolerant Control Applied on Two Inverted Pendulums with Nonaffine Nonlinear Actuator Failures," *International Journal of Robotics and Control Systems*, vol. 3, no. 2, pp. 144-160, 2023, https://doi.org/10.31763/ijrcs.v3i2.917.

[19] C. Xia, I. Qaisar, and M. S. Aslam, "Design of Hybrid Controller using Qualitative Simulation Internal Modeling for Inverted Pendulum," *International Journal of Robotics and Control Systems*, vol. 2, no. 4, pp. 638-651, 2022, https://doi.org/10.31763/ijrcs.v2i4.777.

[20] M. S. Mahmoud, R. A. Saleh, and A. Ma'arif, "Stabilizing of Inverted Pendulum System Using Robust Sliding Mode Control," *International Journal of Robotics and Control Systems*, vol. 2, no. 2, pp. 230-239, 2022, https://doi.org/10.31763/ijrcs.v2i2.594.

[21] N.-C. Tran, "LQR Control for Experimental Double Rotary Inverted Pendulum," *Journal of Fuzzy Systems and Control*, vol. 2, no. 2, pp. 104-108, 2024, https://doi.org/10.59247/jfsc.v2i2.212.

[22] C.-H. Nguyen, "ANFIS-based LQR Control for Rotary Double Parallel Inverted Pendulum," *Journal of Fuzzy Systems and Control*, vol. 2, no. 2, pp. 109-116, 2024, https://doi.org/10.59247/jfsc.v2i2.214.